MSDE

PAPER

View Article Online
View Journal | View Issue

Open Access Article. Published on 24 April 2020. Downloaded on 3/27/2026 3:43:59 AM.
This article is licensed under a Creative Commons Attribution-NonCommercial 3.0 Unported Licence.

Check for updates

Cite this: *Mol. Syst. Des. Eng.*, 2020, **5**, 1071

CO_2 sensing under ambient conditions using metal–organic frameworks†

Bohui Ye,[a] Andreea Gheorghe,[a] Roy van Hal,*[b] Marcel Zevenbergen[b] and Stefania Tanase*[a]

Received 12th January 2020,
Accepted 22nd April 2020

DOI: 10.1039/d0me00004c

rsc.li/molecular-engineering

Determining accurately CO_2 levels is highly relevant when monitoring indoor air quality. Nondispersive infrared (NDIR) sensors are the most often used sensors for measuring carbon dioxide concentration. However, the complexity of the device, power consumption and scalability are the main drawbacks associated with the state-of-the-art devices. In this work, we discuss the application of metal–organic frameworks for sensing of CO_2 molecules using electrochemical impedance spectroscopy. Impedance CO_2 sensors were fabricated using two metal–organic frameworks known for their selective CO_2 adsorption capability as well as their high proton conductivity, namely Zn-MOF-74 and NdMo-MOF. Both sensors showed a significant change in impedance when changing the CO_2 concentration and the relative humidity. Notably, the Zn-MOF-74 impedance sensor showed fast response when changing the humidity and CO_2 concentration.

Design, System, Application

State-of-the-art nondispersive infrared CO_2 sensors are selective and have fast response times but their main drawbacks are related to the device complexity, power consumption and scalability. To overcome these challenges, we propose the use of metal–organic frameworks (MOFs) as effective sensing layers for effective CO_2 level monitoring which can be processed and integrated easily into inexpensive impedance sensors. This work shows that MOFs showing selective CO_2 adsorption and high proton conductivity are suitable sensing materials for integration into electronic sensors with fast and accurate CO_2 response.

Introduction

Excessive CO_2 emissions and global warming require tremendous efforts to address these challenges. Fossil fuels (coal, oil, and natural gas) do substantially more harm than renewable energy sources and they are the main cause of increased emission of CO_2.[1] This is a major environmental concern and therefore, it requires careful monitoring. There are two major types of commercial CO_2 sensors: nondispersive infrared (NDIR) and chemical CO_2 sensors.[2,3] The principle of NDIR sensors is based on the absorption of infrared light at a wavelength characteristic of CO_2. NDIR sensors are selective and have fast response times. They are more stable because they do not suffer from poisoning effects.[4,5] By using selective IR sources or IR filters, the NDIR sensors are very selective, even under a variety of humidity conditions. However, their main disadvantages are their size and power consumption. Cost used to be a drawback as well, but significant progress has been made. Commercial sensors with good selectivity are currently available for <$50 and are expected to become cheaper in the future.[2] Polymer-based sensors for chemical CO_2 detection have been described in the literature. Nevertheless, they have poor selectivity as well as short and long-term sensor drift, leading to inaccurate measurements over time.[6,7] A cost effective alternative would be commercial metal-oxide-based VOC sensors, but they suffer from cross-sensitivity to many components and baseline drift as well as high power consumption because inorganic oxides require high temperatures, *e.g.* 250–350 °C.[8]

Metal–organic frameworks (MOFs) form a class of porous 3D molecular materials.[9,10] Their high surface area to volume ratio is especially beneficial for sensing applications as it enhances the chance of interaction between the sensing materials and analytes, which leads to high sensitivity.[11] In addition, smaller amounts of material are needed to absorb gases as compared to low surface area materials, thereby allowing for the miniaturisation of the sensing layer.[12,13] MOFs are well studied for their potential in CO_2 capture and storage and various MOF structures can be designed to achieve high selectivity towards CO_2.[13] However, much less is known about the potential of MOFs for CO_2 sensing and only very few studies were reported.[14,15] Van Duyne *et al.*[16]

[a] *Van' t Hoff Institute for Molecular Sciences, University of Amsterdam, Science Park 904, 1098 XH Amsterdam, The Netherlands. E-mail: s.grecea@uva.nl*
[b] *Holst Centre, Imec – The Netherlands, P.O. Box 8550, 5605 KN Eindhoven, The Netherlands. E-mail: Roy.vanHal@imec.nl*

† Electronic supplementary information (ESI) available: PXRD, SEM images, and single adsorption isotherms. See DOI:10.1039/d0me00004c

Open Access Article. Published on 24 April 2020. Downloaded on 3/27/2026 3:43:59 AM.
This article is licensed under a Creative Commons Attribution-NonCommercial 3.0 Unported Licence.

fabricated a localized surface plasmon resonance (LSPR) sensor with HKUST-1 and demonstrated the detection of CO_2 levels down to 10% under ambient conditions. Wang *et al.*[17] designed a near-IR optical fibre coated with HKUST-1 that showed a limit of detection of 20 ppm for CO_2. Chocarro-Ruiz *et al.*[18] reported an optical CO_2 sensor by integrating a thin transparent film of ZIF-8 onto a bimodal optical waveguide.

Conductive polymers are associated with low cost and room temperature operation[19,20] and are therefore preferred for the development of low-power gas sensors. As for CO_2 sensing applications, the interaction of CO_2 with conducting polymers is based on either the chemical reactivity or physical adsorption of the target gas.[21] In this respect, MOFs are attractive candidates for CO_2 sensing but studies focusing on the potential integration of MOFs into electronic CO_2 sensing devices are still scarce. Very recently, Kaskel *et al.*[20] have shown that MIL-53(Al)/carbon composites can be used for CO_2 sensing at high temperature whilst Dincă *et al.*[21] have demonstrated the sensing of ambient CO_2 using an imino-based 2D framework. Both studies show that MOFs can provide a powerful platform for chemiresistive sensing of CO_2.

This work demonstrates the potential of MOFs for CO_2 sensing using impedance measurements. It assesses the CO_2 sensing performance of two MOF materials which are known to display significant CO_2 adsorption and have high proton conductivity, namely $[Zn_2(dobdc)(H_2O)_2]\cdot n$solvent (known as Zn-MOF-74, where H_4dobdc = 2,5-dihydroxy-1,4-benzenedicarboxylic acid) and $[Nd(mpca)_2Nd(H_2O)_6Mo(CN)_8]\cdot nH_2O$ (where Hmpca = 5-methyl-2-pyrazinecarboxylic acid), here abbreviated as NdMo-MOF. We discuss the methodology used for their processing as thin-films as well as their performance in CO_2 sensing under ambient conditions.

Results and discussion

In order to use MOFs as sensing layers in a CO_2 sensor, MOFs should be able to selectively adsorb and interact with CO_2 and show a significant change of physical properties upon adsorption and interaction. Because CO_2 is a linear molecule that has a permanent quadrupole moment, this property can be used to selectively adsorb CO_2 from gas mixtures by incorporating open metal sites. The open metal site acts as an attractive site for the CO_2 molecule. Once a CO_2 molecule is adsorbed on the open metal centre, the adsorbed CO_2 molecule acts as an attractive site for other CO_2 molecules, causing a cascade of attractive interactions for the CO_2 molecules. Additionally, CO_2 can react with water molecules to give carbonic acid. This means that if there is lattice water in the MOFs' structure, the change in pH might also be used as a signal for CO_2 sensing. We have selected Zn-MOF-74 (ref. 22 and 23) and NdMo-MOF[24] as representative materials for CO_2 sensing due to their porous 3D structures with open 1D channels (Fig. 1) and metal open sites. In order to be used as a detection layer in an electronic CO_2 sensing device, a MOF needs to possess some electrical conductivity. Conducting[25]

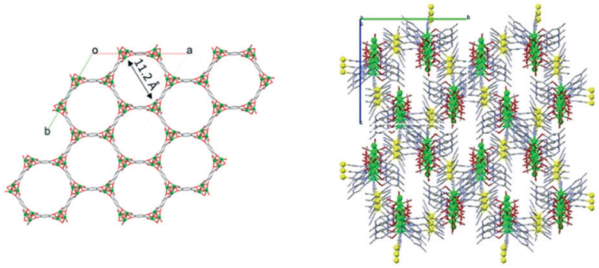

Fig. 1 View of the molecular structures of Zn-MOF-74 (left) and NdMo-MOF (right) showing hydrophilic 1D channels.

and semiconducting[26] MOFs as well as those displaying high proton conductivity[27,28] are suitable for integration into electronic devices. Both Zn-MOF-74 (ref. 29 and 30) and NdMo-MOF[24,31] are known for their very high proton conductivity.

Zn-MOF-74 shows a very high CO_2 uptake due to the presence of three different CO_2 adsorption sites.[22,32,33] As for NdMo-MOF, CO_2 adsorption studies show that this framework is very flexible and a hysteresis loop is observed in the CO_2 adsorption–desorption isotherm.[24] Therefore, we have hypothesised that their CO_2 adsorption behaviour and intrinsic proton conductivity would enable them to be used as sensing layers with a short response time for selective CO_2 detection.

Zn-MOF-74 is also known to have two structural isomers, namely UTSA-74 (ref. 34) and HIMS-74.[35] Although Zn-UTSA-74 has the same number of open metal sites per secondary building unit (SBU) as Zn-MOF-74, a smaller CO_2 uptake is observed for UTSA-74 as compared to MOF-74.[34] The available open sites in HIMS-74 indicate that there are two adsorption sites per SBU, similar to those in UTSA-74, and therefore they show similar CO_2 uptakes. Studying their CO_2 sensing behaviour would have allowed us to make correlations between the type of SBU and the response time of the sensing layer. However, we could not integrate these two materials in a homogeneous sensing layer.

Two MOF-based sensors were prepared using Zn-MOF-74 and NdMo-MOF as sensing layers on a platinum surface using the drop casting method. The main challenges in fabricating thin film MOF-based polymer composites are the aggregation of the MOF nanocrystals and the organic–inorganic incompatibility. Therefore, we have chosen polyvinylpyrrolidone (PVP) as the support for the MOFs due its excellent hydrophilic and surface modification agent properties which facilitate the dispersion of nanoparticles.[36] Moreover, PVP is a nontoxic polymer and its CH_2, CO and C–N functional groups have been widely used to control the shape and nanocrystal size *via* their selective attachment on the specific facets of nanocrystals.[37]

During sensor preparation, NdMo-MOF gave a thin suspension with a high residual content, whereas the sensor with Zn-MOF-74 gave a suspension with a low residual content. The resulting NdMo-MOF sensor had a low MOF

 This journal is © The Royal Society of Chemistry 2020

Open Access Article. Published on 24 April 2020. Downloaded on 3/27/2026 3:43:59 AM.
This article is licensed under a Creative Commons Attribution-NonCommercial 3.0 Unported Licence.

content with a poor particle distribution, whereas the Zn-MOF-74 sensor had a high MOF content with a relatively good particle distribution (see Fig. 2).

CO_2 sensing studies

Prior to the impedance measurements, a frequency sweep was carried out to determine the suitable frequency that gives the optimal signal output. At 10 Hz and 100 Hz, the output signals contain mostly a large amount of noise. At 10 kHz and 100 kHz, the signal is unstable as both impedances showed a high sensor drift. In addition, high frequency also resulted in a low amplitude of the output signals. Thus, we notice that there is a trade-off between the signal noise and the amplitude of the signal.

The assessment of the CO_2 sensing performance of both MOFs was carried out using N_2 as a diluting gas due to its ready availability. The sensing performance of the NdMo-MOF sensor is shown in Fig. 3. Initially, the sensor takes a long time (40 minutes) to reach equilibrium. Impedance changes towards humidity were only observed in the imaginary part, when the relative humidity (RH) was decreased from 60% to 40% after 6 and 15 hours, whereas no clear change in impedance was observed when the RH was changed from 40 to 50% and 50–60%. An impedance change is observed after 4 and 16 hours, when the concentration of CO_2 changes from 0 to 2000 ppm at 60% RH and 40% RH. In addition, the sensor shows a high drift in both the imaginary and real parts of the impedance.

Fig. 4 shows the sensing performance of the Zn-MOF-74-based sensor. Similar to the NdMo-MOF-based sensor, the sensor takes a long time to reach equilibrium during the first cycle (0–3 h). The sensor showed a significant and medium rate of CO_2 adsorption (*ca.* 15 minutes), with slow desorption (>2 h) at all measured RH values. At all measured RH values, changes in both the imaginary and real parts of the impedance are observed upon changing the CO_2 concentration, whereas changing the relative humidity led to an insignificant change in the impedance. This indicates that the Zn-MOF-74-based sensor showed low cross sensitivity.

Additional measurements were carried out with the Zn-MOF-74 sensor at 50% RH, at different CO_2 concentrations (Fig. 5). The sensor showed fast response to CO_2, which is characterised by the increase of the real part of the impedance and the decrease of the imaginary part of the impedance. However, the height of the impedance does not show a clear correlation with the CO_2 concentration. In addition, Fig. 5 shows that the desorption of CO_2 is slow, and the change in impedance is still observable after 6 hours (t = 24–30 h). After finishing the first cycle, the sensor was re-exposed to 500 ppm and 1000 ppm CO_2, which showed a slightly different impedance change compared to the first cycle. This might be due to the stability of the signal levels.

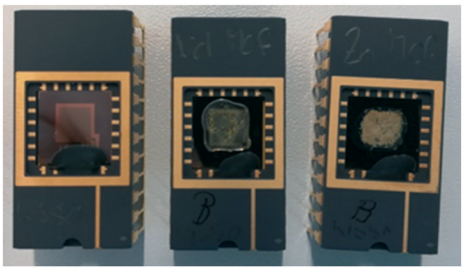

Fig. 2 Sensors prepared for CO_2 sensing, from left to right: pristine sensor, NdMo-MOF-based sensor and Zn-MOF-74 sensor.

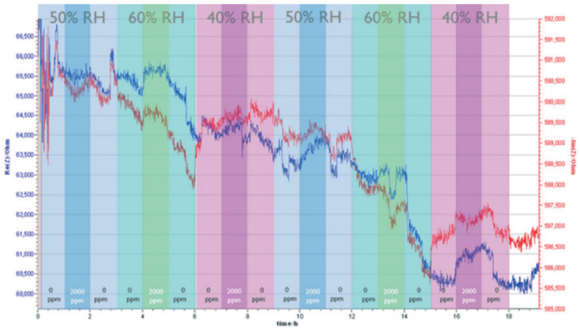

Fig. 3 Performance of the NdMo-MOF-based sensor, by varying the relative humidity and CO_2 concentration.

The following experiments were carried out using synthetic air. During the initial measurement, the sensor is exposed to a CO_2 concentration that alternates between 0 and 1000 ppm every 10 minutes. Then, after 22 hours, the sensor is exposed to synthetic air (80% N_2, 20% O_2), which leads to deactivation of the sensor (Fig. 6, top). To investigate whether the deactivation is permanent, the sensor is exposed again to N_2, and the CO_2 concentration is alternated between 0 and 1000 ppm every 10 minutes. Fig. 6 (bottom) shows that the deactivation of the Zn-MOF-74 sensor is reversible, but it takes more than 1 hour for the sensor to show a response.

Both sensors show fast uptake (10–15 minutes), with a long desorption time (over 2 hours). Hypothetically, the fast uptake of CO_2 might be related to the long desorption time. The stronger the interaction between the metal and CO_2, the harder the release of CO_2 will be from the metal–CO_2 interaction. There should be a trade-off between the fast and selective adsorption and the desorption of CO_2. Therefore, future research will focus on tuning the adsorption and desorption

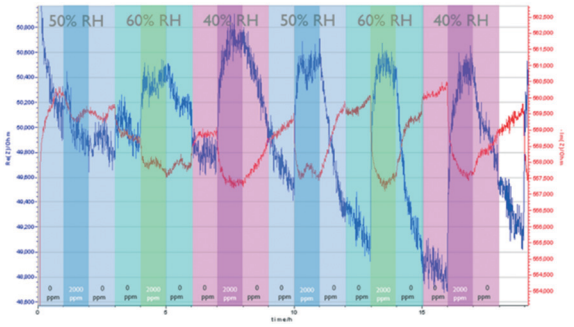

Fig. 4 Performance of the Zn-MOF-74-based sensor, by varying the relative humidity and CO_2 concentration.

Open Access Article. Published on 24 April 2020. Downloaded on 3/27/2026 3:43:59 AM.
This article is licensed under a Creative Commons Attribution-NonCommercial 3.0 Unported Licence.

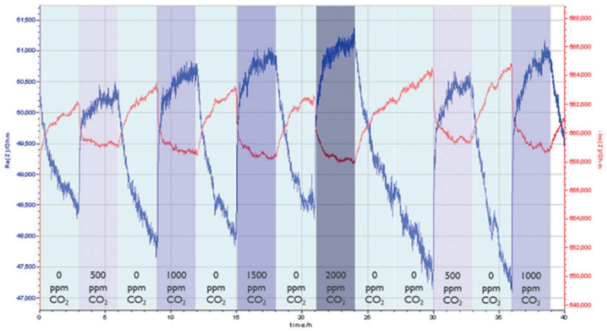

Fig. 5 Performance of the Zn-MOF-74-based sensor at different CO_2 concentrations at 50% RH.

of CO_2, *e.g.* through post-synthetic modification or different strategies involving the choice of metal and linker.[38–40] Alternatively, the CO_2 desorption can be solved through the addition of a heating element to the sensor, allowing for a faster gas release from the MOF's pores.

Both NdMo-MOF and Zn-MOF-74 CO_2 sensors were tested in parallel and no clear indication of the effect of PVP can be deduced from the measurements. PVP is a polymer containing C═O functional groups which might react with water molecules to form dihydroxy groups. However, the potential effect on the impedance is not understood and needs further investigation. This could for example be done by comparing the impedance change of a sensor coated with a PVP layer with that of a pristine sensor. In further studies, the use of organic binders without hydrophilic groups such as polytetrafluoroethylene and polyethylene should further be explored.[41]

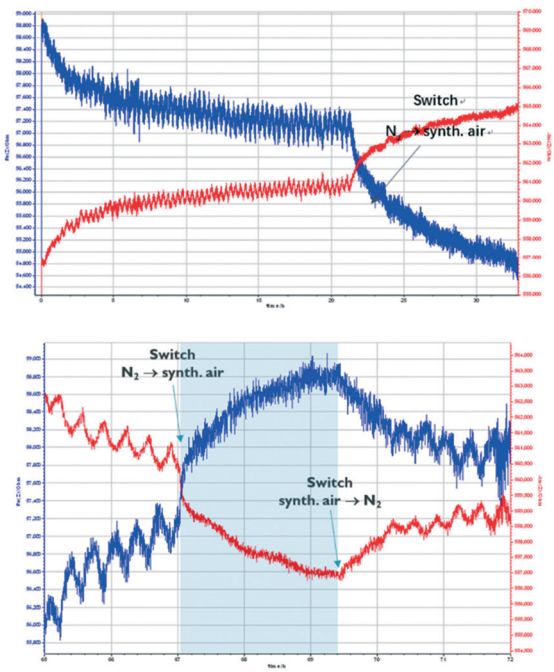

Fig. 6 The effect of diluting gas on the impedance of Zn-MOF-74 measured in N_2 and synthetic air by exposure to CO_2 concentration that alternates between 0 and 1000 ppm every 10 minutes (top) and the reversibility of the deactivation of the Zn-MOF-74-based sensor upon exposure to oxygen in synthetic air (bottom).

Fig. 6 shows the quenching behaviour of oxygen as a diluting gas on the impedance of Zn-MOF-74. The affinity of Pt towards gases such as O_2 (or H_2) is well known,[42] while CO_2 is usually very inert towards metal surfaces. In this regard, the response towards O_2 is to be expected. However, it is noticeable that the Pt, even though it is still conductive, does not pick up the signal from the MOF anymore. At this stage, we have no insight into what is happening at the molecular level. More knowledge will be gained in subsequent research which aims at studying other electrode surfaces, such as gold or non-metallic surfaces.

Our subsequent studies will also aim at investigating the CO_2 sensing properties of the materials in relation to the method used for preparing thin-film MOFs. Typically, thin-film MOFs are fabricated through solvothermal methods, which involve deposition, by dip coating of MOFs on a substrate using the mother solution.[43] Alternatively, thin-film MOFs can be obtained through spray coating of a colloidal solution.[44] For electronic sensing devices, combining MOFs and microfabrication techniques is a key technological advantage because a limited amount of MOF is needed, portability is required, and an integrated multifunctional system is desired. Among various techniques used, the layer-by-layer MOF growth deposition technique leads to high quality SURMOF (surface-mounted metal–organic framework) thin films.[45] The key patterning is the preparation of self-assembled monolayers (SAMs) using liquid-phase epitaxial (LPE) techniques.[46] Currently, we are developing this methodology for the fabrication of NdMo-MOF thin-layers and the results will be published in a subsequent study.

Experimental

Materials and instrumentation

Starting materials, including metal salts, organic linkers and solvents, were purchased from Aldrich and all manipulations were performed using the materials as received. Zn-MOF-74 and NdMo-MOF were synthesised using slightly modified reported procedures.[24,47] Impedance spectroscopy (EIS) measurements were performed using an SP-300 by Bio-Logic Science Instruments (freq. 1.077 kHz, amp. 25 mV, CO_2 0–2000 ppm, relative humidity (RH) 40–60%). Powder X-ray diffraction (PXRD) measurements were carried out on a Rigaku Miniflex X-ray diffractometer. The measurements were conducted in the 5–50° range using a Cu-Kα source. The morphology of the samples with sputtered gold was studied by using a field emission scanning electron microscope (FESEM, FEI Verios 460 scanning electron microscope) operated at 5 kV. N_2 sorption isotherms were measured at 77 K on a Thermo Scientific Surfer. CO_2 adsorption measurements at 273 K were performed on an isothermal Setaram Calvert 80 micro-calorimeter, connected to a home-built manometric apparatus. Zn-MOF-74 was activated by stepwise vacuum heating from RT–100–150–200–270 °C, with a heating rate of

 This journal is © The Royal Society of Chemistry 2020

Open Access Article. Published on 24 April 2020. Downloaded on 3/27/2026 3:43:59 AM.
This article is licensed under a Creative Commons Attribution-NonCommercial 3.0 Unported Licence.

4–2–4–2° min^{-1} and a holding time of 1 h or 12 h for the final step. NdMo-MOF was activated by vacuum heating from RT to 200 °C with a holding time of 2 h.

Synthesis procedures

Zn-MOF-74. 2,5-Dihydroxyterephthalic acid (2.42 mmol, 0.480 g) and $Zn(NO_3)_2{\cdot}6H_2O$ (8.67 mmol, 2.579 g) were dissolved in a mixed solvent of DMF : ethanol : water (1 : 1 : 1, v/v/v%, 200 mL) solution. The suspension was stirred for 10 minutes at room temperature to obtain a clear solution, which was then placed in an oven at 100 °C for 24 h. After cooling to room temperature, the supernatant was separated from the precipitate through filtration with paper. The precipitate was washed three times with methanol and immersed in 50 mL methanol, which was replenished four times in two days. The solvents were removed through filtration and dried in an oven at 80 °C overnight, after which rod-like crystals were obtained.

NdMo-MOF. $Nd(NO_3)_3{\cdot}6H_2O$ (2.00 mmol, 0.876 g) and 5-methylpyrazine-2-carboxylic acid (4.00 mmol, 0.552 g) were dissolved in 12 mL demineralized water. In a separate beaker, $K_4[Mo(CN)_8]{\cdot}2H_2O$ (2.00 mmol, 0.992 g) was dissolved in 12 mL demineralized water. The solutions were combined and stirred for five minutes. Then 2 mL of the combined solution was added to eight tubes containing 6 mL methanol each, so that all the tubes had a total volume of 8 mL. The tubes were wrapped in aluminium foil and placed in the dark for four days at room temperature. The solids were isolated through paper filtration, and washed three times with 30 mL methanol and three times with 30 mL demineralized water. The solids were collected and dried in the dark under a N_2 atmosphere at 35 °C.

Fabrication of the impedance sensor. 25 mg of finely powdered MOF (Zn-MOF-74 and NdMo-MOF) were suspended in 500 mg deionized water. The mixture was sonicated for 20 minutes. 15 μL of 1% polyvinylpyrrolidone (PVP) solution was deposited onto the sensor surface (provided by IMEC). 15 μL of MOF suspension was added and mixed by stirring with an Eppendorf tip. The sensors were placed in an oven and dried at 80 °C overnight.

Conclusions

This work demonstrates the potential of MOFs for gas sensing applications using impedance measurements. These MOFs offer significant advantages as compared with state-of-the-art MOFs for CO_2 sensing, which is based on chemical resistance studies. Chemiresistive sensing requires conductive MOFs which are difficult to synthesise whilst measuring impedance changes requires only a small current change, *e.g.* easily achieved with proton conductive MOFs. Using this approach, two MOF sensors (NdMo-MOF and Zn-MOF-74) were prepared through drop casting of the MOF suspension on a platinum surface and their CO_2 sensing properties were evaluated based on impedance measurements. Both sensors showed drift, which increases over time. Upon exposure to changing CO_2 concentration and relative humidity, both MOF-based sensors showed changes in impedance. The Zn-MOF-74-based sensor showed fast response towards a change in the relative humidity and CO_2 concentration. Increasing the CO_2 concentration leads to an increase of the impedance (both real and imaginary). Further analysis of the diluting gas showed the quenching effect of O_2 on the change in impedance. CO_2 adsorption, storage and detection are of significant interest for many industrial processes and climate related topics. With the expanding library of the MOF literature, MOFs for CO_2 sensing could benefit from this expansion. There are only a few studies reporting on the use of MOFs for CO_2 sensing. Most of these studies reported sensors which often required large equipment to detect CO_2. Impedance sensors, similar to those discussed by us, have the advantage that they can be integrated into compact and portable devices. Therefore, we foresee that more studies will be focused on evaluating the potential of MOFs for portable sensors with different signal transduction pathways.

Conflicts of interest

There are no conflicts to declare.

Acknowledgements

This work is part of the Research Priority Area Sustainable Chemistry of the University of Amsterdam, http://suschem.uva.nl.

Notes and references

1 D. D. Zhu, J. L. Liu and S. Z. Qiao, *Adv. Mater.*, 2016, **28**, 3423–3452.
2 K. Kalwinder, *Carbon Dioxide Sensor*, AZoSensors, 2013, https://www.azosensors.com/article.aspx?ArticleID=234.
3 S. Neethirajan, D. S. Jayas and S. Sadistap, *Food Bioprocess Technol.*, 2009, **2**, 115–121.
4 S. You-Wen, Y. Zeng, W.-Q. Liu, P.-H. Xie, K.-L. Chan, X.-X. Li, S.-M. Wang and S.-H. Huang, *Chin. Phys. B*, 2012, **21**, 168–175.
5 T.-V. Dinh, I.-Y. Choi, Y.-S. Son and J.-C. Kim, *Sens. Actuators, B*, 2016, **231**, 529–538.
6 S. Srinives, T. Sarkar, R. Hernandez and A. Mulchandani, *Anal. Chim. Acta*, 2015, **874**, 54–58.
7 X. Liu, S. Cheng, H. Liu, S. Hu, D. Zhang and H. Ning, *Sensors*, 2012, **12**, 9635–9665.
8 S. Achmann, G. Hagen, J. Kita, I. M. Malkowsky, C. Kiener and R. Moos, *Sensors*, 2009, **9**, 1574–1589.
9 C. Wang, D. Liu and W. Lin, *J. Am. Chem. Soc.*, 2013, **135**, 13222–13234.
10 O. K. Farha and J. T. Hupp, *Acc. Chem. Res.*, 2010, **43**, 1166–1175.
11 R. Pohle, A. Tawil, P. Davydovskaya and M. Fleischer, *Procedia Eng.*, 2011, **25**, 108–111.
12 H. Yoon, *Nanomaterials*, 2013, **3**, 524–549.
13 M. D. Allendorf, A. Schwartzberg, V. Stavila and A. A. Talin, *Chem. – Eur. J.*, 2011, **17**, 11372–11388.
14 M. P. Batten, M. Rubio-Martinez, T. Hadley, K.-C. Carey, K.-S. Lim, A. Polyzos and M. R. Hill, *Curr. Opin. Chem. Eng.*, 2015, **8**, 55–59.

Open Access Article. Published on 24 April 2020. Downloaded on 3/27/2026 3:43:59 AM.
This article is licensed under a Creative Commons Attribution-NonCommercial 3.0 Unported Licence.

15 L. E. Kreno, K. Leong, O. K. Farha, M. Allendorf, R. P. Van Duyne and J. T. Hupp, *Chem. Rev.*, 2012, **112**, 1105–1125.
16 L. E. Kreno, J. T. Hupp and R. P. Van Duyne, *Anal. Chem.*, 2010, **82**, 8042–8046.
17 X. Chong, K.-J. Kim, E. Li, Y. Zhang, P. R. Ohodnicki, C.-H. Chang and A. X. Wang, *Sens. Actuators, B*, 2016, **232**, 43–51.
18 B. Chocarro-Ruiz, J. Pérez-Carvajal, C. Avci, O. Calvo-Lozano, M. Isabel Alonso, D. Maspoch and L. M. Lechuga, *J. Mater. Chem. A*, 2018, **6**, 13171–13177.
19 H. Bai and G. Shi, *Sensors*, 2007, **7**, 267–307.
20 P. Freund, L. Mielewczyk, M. Rauche, I. Senkovska, S. Ehrling, E. Brunner and S. Kaskel, *ACS Sustainable Chem. Eng.*, 2019, **7**, 4012–4018.
21 I. Stassen, J.-H. Dou, C. Hendon and M. Dincă, *ACS Cent. Sci.*, 2019, **5**, 1425–1431.
22 X. Kong, E. Scott, W. Ding, J. A. Mason, J. R. Long and J. A. Reimer, *J. Am. Chem. Soc.*, 2012, **134**, 14341–14344.
23 V. Pentyala, P. Davydovskaya, R. Pohle, G. Urban and O. Yurchenko, *Procedia Eng.*, 2014, **87**, 1071–1074.
24 S. Tanase, M. C. Mittelmeijer-Hazeleger, G. Rothenberg, C. Mathonière, V. Jubera, J. M. M. Smits and R. de Gelder, *J. Mater. Chem.*, 2011, **21**, 15544–15551.
25 C.-W. Kung, K. Otake, C. T. Buru, S. Goswami, Y. Cui, J. T. Hupp, A. M. Spokoyny and O. K. Farha, *J. Am. Chem. Soc.*, 2018, **140**, 3871–3875.
26 K. Naskar, A. Dey, B. Dutta, F. Ahmed, C. Sen, M. H. Mir, P. P. Roy and C. Sinha, *Cryst. Growth Des.*, 2017, **17**, 3267–3276.
27 P. Ramaswamy, N. E. Wong, B. S. Gelfand and G. K. H. Shimizu, *J. Am. Chem. Soc.*, 2015, **137**, 7640–7643.
28 X.-S. Xing, Z.-H. Fu, N.-N. Zhang, X.-Q. Yu, M.-S. Wang and G.-C. Guo, *Chem. Commun.*, 2019, **55**, 1241–1244.
29 S. Hwang, E. J. Lee, D. Song and N. C. Jeong, *ACS Appl. Mater. Interfaces*, 2018, **10**, 35354–35360.
30 W. J. Phang, W. R. Lee, K. Yoo, D. W. Ryu, B. Kim and C. S. Hong, *Angew. Chem., Int. Ed.*, 2014, **53**, 8383–8387.
31 Y. Gao, P. Jing, N. Yan, M. Hilbers, H. Zhang, G. Rothenberg and S. Tanase, *Chem. Commun.*, 2017, **53**, 4465–4468.
32 W. L. Queen, M. R. Hudson, E. D. Bloch, J. A. Mason, M. I. Gonzalez, J. S. Lee, D. Gygi, J. D. Howe, K. Lee, T. A. Darwish, M. James, V. K. Peterson, S. J. Teat, B. Smit, J. B. Neaton, J. R. Long and C. M. Brown, *Chem. Sci.*, 2014, **5**, 4569–4581.
33 H. Kim, M. Sohail, K. Yim, Y. C. Park, D. H. Chun, H. J. Kim, S. O. Han and J.-H. Moon, *ACS Appl. Mater. Interfaces*, 2019, **11**, 7014–7021.
34 F. Luo, C. Yan, L. Dang, R. Krishna, W. Zhou, H. Wu, X. Dong, Y. Han, T.-L. Hu, M. O'Keeffe, L. Wang, M. Luo, R.-B. Lin and B. Chen, *J. Am. Chem. Soc.*, 2016, **138**, 5678–5684.
35 A. Gheorghe, I. Imaz, J. I. van der Vlugt, D. Maspoch and S. Tanase, *Dalton Trans.*, 2019, **48**, 10043–10050.
36 P. Zhao, R. Li, W. Wu, J. Wang, J. Liu and Y. Zhang, *Composites, Part B*, 2019, **176**, 107208.
37 S. Chandra Sahu, A. K. Samantara, B. Satpati, S. Bhattacharjee and B. Kumar Jena, *Nanoscale*, 2013, **5**, 11265–11274.
38 X. Su, L. Bromberg, V. Martis, F. Simeon, A. Huq and T. A. Hatton, *ACS Appl. Mater. Interfaces*, 2017, **9**, 11299–11306.
39 M. Gholami and S. Yeganegi, *Adsorption*, 2017, **23**, 507–514.
40 Y. Jiao, C. R. Morelock, N. C. Burtch, W. P. Mounfield, J. T. Hungerford and K. S. Walton, *Ind. Eng. Chem. Res.*, 2015, **54**, 12408–12414.
41 F. M. Delnick, A. Iwamoto, Z. Hu and L. Wang, *US* 6316142B1, 2001.
42 R. Lewis and R. Gomer, *Surf. Sci.*, 1968, **12**, 157–176.
43 A. Bétard and R. A. Fischer, *Chem. Rev.*, 2012, **112**, 1055–1083.
44 B. Hoppe, K. D. J. Hindricks, D. P. Warwas, H. A. Schulze, A. Mohmeyer, T. J. Pinkvos, S. Zailskas, M. R. Krey, C. Belke, S. König, M. Fröba, R. J. Haug and P. Behrens, *CrystEngComm*, 2018, **20**, 6458–6471.
45 O. Shekhah, *Materials*, 2010, **3**, 1302–1315.
46 J. Liu, O. Shekhah, X. Stammer, H. K. Arslan, B. Liu, B. Schüpbach, A. Terfort and C. Wöll, *Materials*, 2012, **5**, 1581–1592.
47 S. R. Caskey, A. G. Wong-Foy and A. J. Matzger, *J. Am. Chem. Soc.*, 2008, **130**, 10870–10871.

 This journal is © The Royal Society of Chemistry 2020